



University of Southern Denmark

Synthesis and Structural Characterization of a Pure $\text{ZnAl}_4(\text{OH})_{12}(\text{SO}_4)_2 \cdot 2.6\text{H}_2\text{O}$ Layered Double Hydroxide

Jensen, Nicholai Daugaard; Duong, Nghia Tuan; Bolanz, Ralph; Nishiyama, Yusuke; Rasmussen, Camilla Aistrup; Gottlicher, Jorg; Steininger, Ralph; Prevot, Vanessa; Nielsen, Ulla Gro

Published in:
Inorganic Chemistry

DOI:
10.1021/acs.inorgchem.9b00390

Publication date:
2019

Document version:
Accepted manuscript

Citation for polished version (APA):

Jensen, N. D., Duong, N. T., Bolanz, R., Nishiyama, Y., Rasmussen, C. A., Gottlicher, J., Steininger, R., Prevot, V., & Nielsen, U. G. (2019). Synthesis and Structural Characterization of a Pure $\text{ZnAl}_4(\text{OH})_{12}(\text{SO}_4)_2 \cdot 2.6\text{H}_2\text{O}$ Layered Double Hydroxide. *Inorganic Chemistry*, 58(9), 6114-6122.
<https://doi.org/10.1021/acs.inorgchem.9b00390>

Go to publication entry in University of Southern Denmark's Research Portal

Terms of use

This work is brought to you by the University of Southern Denmark.
Unless otherwise specified it has been shared according to the terms for self-archiving.
If no other license is stated, these terms apply:

- You may download this work for personal use only.
- You may not further distribute the material or use it for any profit-making activity or commercial gain
- You may freely distribute the URL identifying this open access version

If you believe that this document breaches copyright please contact us providing details and we will investigate your claim.
Please direct all enquiries to puresupport@bib.sdu.dk

Synthesis and structural characterization of a pure $\text{ZnAl}_4(\text{OH})_{12}(\text{SO}_4)\cdot 2.6 \text{ H}_2\text{O}$ layered double hydroxide

Nicholai Daugaard Jensen¹, Nghia Tuan Duong², Ralph Bolanz³, Yusuke Nishiyama^{2,4,5}, Camilla Aistrup Rasmussen¹, Jorg Gottlicher⁶, Ralph Steininger⁶, Vanessa Prevot,⁷ and Ulla Gro Nielsen^{1,*}

¹ Department of Physics, Chemistry, and Pharmacy, University of Southern Denmark, Campusvej 55, 5230 Odense M, Denmark

² RIKEN-JEOL Collaboration Center, RIKEN, Yokohama, Kanagawa 230-0045, Japan

³ Friedrich-Schiller-University, Institute of Geosciences, Carl-Zeiss-Promenade 10, 07745 Jena, Germany

⁴ NMR Science and Development Division, RIKEN SPring-8 Center, Tsurumi, Yokohama, Kanagawa 230-0045, Japan

⁵ JEOL RESONANCE Inc., Musashino, Akisma, Tokyo 186-8558, Japan

⁶ Karlsruhe Institute of Technology, Institute for Photon Science and Synchrotron Radiation (IPS), Hermann-vn-Helmholtz Platz 1, D-79344 Eggenstein-Leopoldshafen, Germany

⁷ Université Clermont Auvergne, CNRS, SIGMA Clermont, ICCF, F-63000 Clermont-Ferrand, France

Abstract

The phase purity of a series of $\text{ZnAl}_4(\text{OH})_{12}\text{SO}_4 \cdot n\text{H}_2\text{O}$ layered double hydroxides (ZnAl₄-LDH) obtained from a reaction of bayerite ($\text{Al}(\text{OH})_3$) with an excess of zinc(II) sulfate under hydrothermal conditions was investigated as a function of the reaction temperature, the duration of the hydrothermal treatment, and the zinc(II) concentration. The product quality, i.e., crystalline impurities, Al impurities and bulk Zn:Al ratio, were assessed by powder X-ray diffraction (PXRD), ^{27}Al MAS NMR, and elemental analysis. Structural characterization of a stoichiometric ZnAl₄-LDH (120 °C, 9 days, and 2.8 M Zn(II)) showed a well-defined structure of the metal ion layer as evident by a single, well-defined Zn environment, i.e., no Zn substitution on the Al sites according to Zn *K*-edge EXAFS and PXRD. Furthermore, nearly all of the twelve different ^1H in the -OH groups and 4 ^{27}Al resonances could be assigned using ^1H , ^{27}Al NMR correlation experiments recorded with ultra-fast MAS. The interlayer water content is variable based thermogravimetric analysis and changes in the ^1H MAS NMR spectra with temperature. A composition of $\text{ZnAl}_4(\text{OH})_{12}(\text{SO}_4) \cdot 2.6\text{H}_2\text{O}$ was obtained from combination of these techniques and confirmed that ZnAl₄-LDH is isostructural to the mineral nickelalumite ($\text{NiAl}_4(\text{OH})_{12}\text{SO}_4 \cdot 3\text{H}_2\text{O}$).

Keywords: layered double hydroxides, bayerite, hydrothermal treatment, solid state NMR spectroscopy, powder X-ray diffraction, competitive reactions

Introduction:

Layered double hydroxides (LDH) are a large class of inorganic minerals and materials, which find wide spread application due to properties as anion exchange materials and reactivity. The most commonly studied are the hydrotalcite-like LDH due to their facile synthesis and functionalization.¹

These are obtained by substitution of one sixth to one third of the divalent cations in a layered M(II) hydroxide, $M(OH)_2$, by a trivalent cation, which is accompanied by insertion of an anion for charge balance and a variable amount of interlayer water, i.e., a chemical composition of $M(II)_{1-x}M(III)_x(OH)_2A_n \cdot nH_2O$ with $1/6 \leq x \leq 1/3$ and $n \approx 2-3$. A second class of LDH is obtained by incorporation of lithium and divalent metal ions into the aluminum hydroxides ($Al(OH)_3$) bayerite and gibbsite, whereby all and half of the vacancies in the dioctahedral layers are filled as illustrated in Figure 1 for Zn(II), accompanied by insertion of an anion. $M(II)Al_4$ -LDH have a high affinity for tetrahedral anions.² Insertion of Li^+ in gibbsite and bayerite proceeds under mild condition and these so-called LiAl-LDH materials have been widely studied.³⁻⁶ In contrast, incorporation of divalent cations such as Mg^{2+} , Zn^{2+} , Co^{2+} , and Ni^{2+} requires excess metal salts and hydrothermal conditions,⁷⁻¹⁴ where dehydroxylation of the $Al(OH)_3$ may compete with formation of the target MAl_4 -LDH, as observed for $ZnAl_4$ -LDH.¹¹ Their chemical structure is closely related to that of the minerals nickelalumite ($NiAl_4(OH)_{12}SO_4 \cdot 3H_2O$)² and chalcoalumite ($CuAl_4(OH)_{12}SO_4 \cdot 3H_2O$).¹⁵ The challenging synthesis conditions for MAl_4 -LDH have hampered their structural characterization and property test as interference with both amorphous and crystalline impurities as well as the low crystallinity of the targeted MAl_4 -LDH has a significant impact on the analysis. The two property studies investigated isomer selective interaction with organic acids¹⁶ by MAl_4 -LDH prepared from gibbsite ($M = Zn, Co, Ni, \text{ and } Cu$) and the relative affinity for simple inorganic anions in ion-exchange experiments.^{9, 14} The reader is referred to Pushparaj et al.¹¹ for a detailed review of the limited literature on $M(II)Al_4$ -LDH and the structural differences between $M(II)Al_4$ -LDH and hydrotalcite-LDH.

To our knowledge, only three studies of synthetic MAl_4 -LDH have provided detailed structural insight (crystal structure). Britto and Kamath obtained a structure of $ZnAl_4$ -LDH with sulfate from Rietveld refinement of powder X-ray diffraction (PXRD) data combined with elemental analysis.⁸

However, their sample contained excess Zn (Al:Zn \approx 3:1), which was modelled as Zn substitution on one of the four crystallographic Al sites and with substantial Zn/Al vacancies.⁸ Williams et al. reported the structure of ZnAl₄-LDH with nitrate, but the sample was heated at 175 °C to remove interlayer water,¹⁴ and a number of structural ambiguities remain.^{14, 17} Recently, Pushparaj et al.¹¹ reported a Rietveld refined structure of a ZnAl₄-LDH sample, which contained no crystalline impurities according to PXRD. Several structural models were validated using input from ²⁷Al solids-state NMR spectroscopy (SSNMR) and transmission electron microscopy (TEM). Elemental analysis showed ca 20 % excess Al in the samples primary in the form of boehmite (AlOOH). Chitrakar et al.⁹ indexed the PXRD diffractogram of a pure MgAl₄-LDH with an orthorhombic unit cell, but no unit cell parameters were given. Thus, synthesis of a pure MA₄-LDH, which have been confirmed by detailed structural characterization has not been reported to our knowledge.

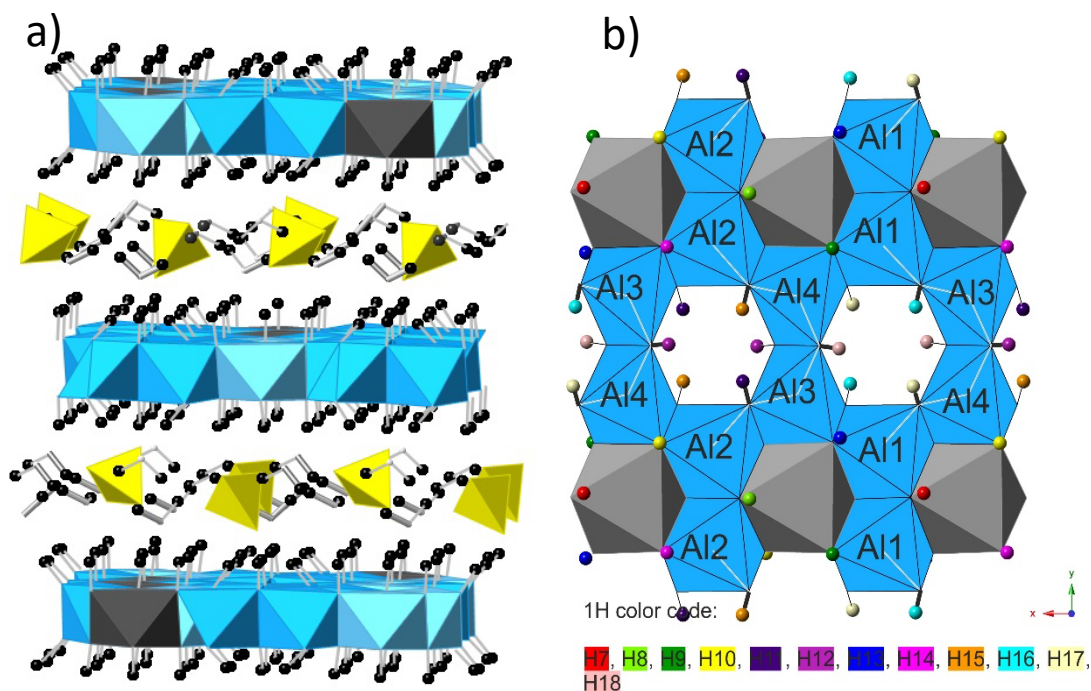


Figure 1. a) The nickelaluminate structure,² which ZnAl₄-LDH crystallizes in, and b) the cation layer with the four crystallographic Al and 12 -OH groups color coded according to the reported crystal structure of nickelaluminate.² The -OH bonds above and below the cation layer are shown with — and —, respectively

Our previous study showed that dehydration of bayerite to form boehmite competes with ZnAl₄-LDH formation at temperatures above 130 °C with a reaction time of two days, whereas lower reaction temperatures resulted in an incomplete reaction without formation of boehmite.¹¹ The original synthesis⁸ used a nearly twenty fold excess of the zinc salt as compared to bayerite, which is costly and generates a lot of waste.

In this study we present the results from a detailed synthesis optimization, which lead to the preparation of pure, stoichiometric ZnAl₄-LDH with sulfate in the interlayer as well as insight into how different synthesis parameters influences the sample purity. A stoichiometric sample was subject to a detailed structural analysis of the experimental data obtained from PXRD, Zn K-edge extended X-ray absorption fine structure (EXAFS), 1D and 2D ¹H and ²⁷Al solid state NMR (SSNMR) experiments, thermogravimetric analysis (TGA), and transmission electron microscopy

(TEM). This provided detailed insight into the structure of this material from the atomic level to the bulk. Furthermore, the limit of SSNMR for assignment of inorganic materials was tested, as ZnAl₄-LDH contains four Al and eighteen crystallographic inequivalent H, respectively.

Experimental section

Materials Synthesis: Aluminum chloride hexahydrate (AlCl₃·6H₂O, 99.0 ≥ Sigma-Aldrich), zinc sulfate hepta-hydrate (ZnSO₄·7H₂O, 99.0 ≥ Sigma-Aldrich), 25% ammonia solution (25% NH₄OH). All chemicals, which were reagent grade, were used without further purifications and MilliQ water was used throughout. The exact water content of the metal salts was determined by thermal gravimetric analysis (TGA) prior to synthesis.

Bayerite was prepared by the method of K. R. Poeppelmeier and S. J. Hwu¹⁸ and similar to our earlier study except that the synthesis was scaled by a factor of five.¹¹ 20.28 g (152.1 mmol) AlCl₃·6H₂O was dissolved in 300 mL water. Subsequently, 21.8 mL of a 25 wt% ammonia solution was added (3 mL/min) followed by addition of 224 mL of a 15 % ammonia solution to ensure a pH above 11. The solution was aged overnight without stirring. The solid product was isolated by centrifugation (10,000 rpm, 5 min) and washed with 250 mL MilliQ water. The washing was repeated thrice, at which point all chloride had been removed (tested by addition of 1 M silver nitrate to the supernatant). The sample purity was checked by PXRD, ICP-OES, and ²⁷Al SSNMR.

ZnAl₄-LDHs were prepared by hydrothermal treatment of bayerite in a zinc sulfate solution as previously described¹¹ using autoclaves with a volume of 40 mL and 80 mL, respectively. It is important that all zinc sulfate is dissolved prior to addition of bayerite, for this heating may be needed. The autoclave was filled to half of the maximum volume with the zinc sulfate solution, then 0.25 g and 0.50 g of bayerite was added to the 40 mL and 80 mL autoclaves, respectively. The durations and temperature of the hydrothermal treatment combined with the concentrations of the

zinc sulfate solution are summarized in Table S1. The reaction mixture was centrifuged to separate the solid product, which was subsequently washed with MilliQ water thrice, and then dried at 65 °C overnight.

Powder X-ray diffraction (PXRD) diffractograms were recorded on a Rigaku Miniflex 600 with a Cu K α ($\lambda=1.54058$ Å) radiation from $2\Theta = 3$ to 70° with a step size of 0.02° and a scanning rate of $10^\circ/\text{min}$. The diffractograms were analyzed using PXL2 and full Rietveld refinements were performed of the pure sample (120-9x20) using the program TOPAS and the structure of nickelalumite,² in which Zn has an occupancy of 1. For each fit, the statistical measures of the deviation of the fit from the obtained data are given in brackets, including the residuals for the weighted profile (R_{wp}) and the goodness-of-fit (GOF). Sites marked with an asterisk were not refined. The crystallite size, which corresponds to the average size of coherent scattering domains, was calculated during the full-profile fit with the software TOPAS® using a Lorentzian function. The PXRD diffractograms were simulated with the software Profex V3.10.2.¹⁹

Bulk chemical composition (Metal ion content and thermogravimetric analysis): Inductive coupled plasma-optical emission spectroscopy (ICP-OES) was used to determine the Zn and Al content. Approximately 10 mg of sample was dissolved in concentrated nitric acid prior to analysis. Thermogravimetric analysis was performed on a Perkin-Elmer thermal gravimetric analyzer (TGA) for selected samples using approximately 10 mg of the sample. The sample was heated to 900°C with a rate of $10^\circ\text{C}/\text{min}$.

Extended X-ray absorptions fine spectroscopy (EXAFS):

EXAFS spectra of sample ZnAl₄-120-9x2.8 (ZnAl₄-LDH) were collected at the Zn K-edge (9659 eV) at the SUL-X beamline of the Karlsruhe Research Accelerator (KARA), Germany. The sample was pressed into a cellulose pellet. For optimum absorption, a defined mass of each sample

was calculated using the software XAFSmass²⁰ and subsequently mixed with cellulose powder, homogenized, and pressed to pellets.

The spectra at the Zn *K*-edge were collected with a step width of 5 eV in the region -150 to -50 eV, 1 eV in the region -50 to -20 eV below the edge, 0.3 eV in the region -20 to +20 eV relative to the edge, and with *k* step widths of 0.05 Å⁻¹ up to *k* 18 Å⁻¹ (about 1230 eV) above the absorption edge. All spectra were measured simultaneously in transmission and fluorescence mode. A Zn metal foil was mounted between ionization chamber 2 and 3 and the Zn *K*-edge was recorded parallel to each sample spectrum for energy calibration. Five spectra were measured for the sample ZnAl₄-120-9x2.8 to get a good signal to noise ratio.

All EXAFS spectra were processed and fit by the Athena and Artemis software packages.²¹ For the “shell-by-shell” fitting of the *k*³-weighted EXAFS spectra, we used paths generated from the model of nickelalumite² for the first and second shell, where Ni was completely substituted by Zn. Parameters for the paths were calculated by FEFF6²² embedded in the Artemis software package. For the fit, the statistical measures of the deviation of the fit from the obtained data are given, including the number of variables allowed to float in the fit (*N*_{var}), number of independent data points (*N*_{idp}), and the *R* factor. The *N*_{idp} is equal to 2Δ*kR*/π where *k* and *R* are the fitting ranges. The *R* factor is defined as:

$$R = \frac{\sum[\chi_i^{data} - \chi_i^{model}(x)]^2}{\sum[\chi_i^{data}]^2}$$

where χ is the magnitude of the EXAFS oscillations and *x* is the set of variables to be refined. Multiple scattering (MS) oscillations for the oxygen atoms of the first shell were also included in the fit. The variable Δ*r* of the MS-path (Δ*r*_{Zn-O-O-Zn}) was assumed to be twice the value of the variable Δ*r*_{Zn-O-Zn} of the first shell, in which Δ*r*_{Zn-O-Zn} was refined. Similarly, the variable σ² of the MS-paths (σ²_{Zn-O-O-Zn}) was also assumed to be twice the value of σ²_{Zn-O-Zn} of the first shell.

Solid-State NMR spectroscopy:

Initial screening of the samples was assessed by single pulse ^{27}Al MAS and 3QMAS (three-pulse, z-filter sequence²³) experiments on an Agilent INOVA 600 spectrometer (14.1 T) using a 3.2 mm triple resonance MAS NMR probe and 15 kHz spinning speed. Single pulse NMR spectra were recorded with a short flip angle to ensure quantitative spectra. Detailed characterization of the pure $\text{ZnAl}_4\text{-LDH}$ sample was performed on a 500 MHz Oxford magnet (11.7 T) equipped with a JEOL Resonance ECZ 500R console, a JNM-ECZ600R (JEOL RESONANCE Inc., 14.1 T) and a JNM-ECZ900R (21.1 T) solid-state NMR spectrometers using a 1 mm $^1\text{H}/\text{X}$ double resonance, 0.75 mm $^1\text{H}/\text{X}$ double-resonance, and a 0.75 mm $^1\text{H}/^{13}\text{C}/^{15}\text{N}$ triple-resonance probes, respectively. The sample temperature was maintained at about 25 °C at 14.1 and 21.1 T by cooling of the VT gas to 10 °C to avoid dehydration due to frictional heating caused by the fast MAS speeds. The lengths of 90° and 180° pulses (t_{90} , t_{180}) for ^1H were set to (1.7, 3.5), (0.75, 1.5) μs and (0.6, 1.2) μs for 500, 600 MHz, and 900 MHz spectrometers, respectively.

^1H - ^1H correlation experiments (NOESY): Experiments were carried out at ultra-high field (900 MHz) and with ultra-fast MAS (80 kHz) to ensure the best resolution in the ^1H NMR spectra. The proton correlations were probed by the two-dimensional (2D) Nuclear Overhauser effect spectroscopy (NOESY) using 12 scans, a relaxation delay of 1 s, with 256 t_1 increments (20 kHz spectral width in the indirect dimension) and different mixing times (1, 2, 5, and 10 ms).

Dipolar-mediated ^1H - ^{27}Al correlations probed by 2D NMR spectroscopy: Dipolar-mediated²⁴⁻²⁶ proton-detected heteronuclear multiple quantum coherence (*D*-HMQC) experiments were performed at 14.1 T (600 MHz) and at a MAS frequency of 80 kHz. A $\text{SR}4_1^2$ recoupling sequence,²⁷ which is a super cycled version of $\text{R}4^2_1\text{R}4^{-2}_1$ was employed to reintroduce the dipolar coupling of the ^1H - ^{27}Al pairs. One loop of $\text{R}4^2_1\text{R}4^{-2}_1$, lasting for 25 μs , was used for both excitation and reconversion durations. A short ^{27}Al pulse length (0.7 μs) ensured excitation of the satellite transitions. Rotor-synchronized acquisition in the indirect dimension folded the spinning sidebands

onto the center band. These 2D spectra were recorded with a recycle delay of 0.7 s, 192 scans, 128 t_1 increments spaced by 12.5 μ s (80 kHz spectral width in the F1 dimension). A $^1\text{H},^{27}\text{Al}$ HETCOR spectrum was recorded on a Bruker NMR spectrometer at 22.3 T (950 MHz for ^1H) using a 2.5 mm HX MAS probe (35 kHz spinning) with a 0.5 ms contact time to probe short $^1\text{H}-^{27}\text{Al}$ distances, a recycle delay of 1 s, 256 scans, and 128 t_1 increments were collected.

Water ($\delta_{\text{iso}}(^1\text{H}) = 4.6$ ppm) and 1 M AlCl_3 ($\delta_{\text{iso}}(^{27}\text{Al}) = 0.0$ ppm) were used as external references. The SSNMR data were analyzed using VNMRJ 4.2, Delta 5.05, MestReNova 6.1.1, and QuadFit.²⁸

TEM:

TEM images were obtained using a Hitachi 7650 microscope at an acceleration voltage of 80 kV. The samples were dispersed in ethanol by stirring for 1 h. A single droplet of the suspension was deposited on a 400 mesh holey carbon-coated copper grid and left to dry in air.

Results and discussion

Synthesis optimization: The sample quality (purity) was systematically assessed by PXRD, ^{27}Al NMR, and ICP-OES, which provided insight into the crystalline phases, the amorphous and crystalline Al phases (ZnAl_4 -LDH, bayerite, and boehmite) and bulk Zn:Al ratio, as these techniques were available in house.

From our extensive optimizations (Table S1, Figure S1, and Ref¹¹), it is clear that the reaction temperature and thereby duration of the hydrothermal treatment is the most important variable. Moreover, the volume of the autoclave also seems to influence the product purity. Our result shows that the dehydroxylation of bayerite competes with formation of ZnAl_4 -LDH above 120 °C, c.f., Table S1 and Figure 2. Thus, we fixed the reaction temperature at 120 °C and studied the effect of the reaction time varying this from one to eleven days. Reaction times of nine, ten, and eleven days all result in samples with 80 mole% Al (stoichiometric within experimental uncertainties), no

crystalline impurities according to PXRD, and ^{27}Al MAS spectra that could be simulated without bayerite and/or boehmite impurities. The original synthesis requires a large excess of zinc sulfate, which is undesirable from an environmental point. Thus, the amount of Zn(II) sulfate was varied from stoichiometric (Zn:Al molar ratio of 1:4) to a 17 fold excess (Zn:Al = 17:1). It was evident that at least a ten-fold excess of zinc(II) sulfate was needed to ensure formation of a pure product within a reasonable reaction time (about 9 days) otherwise an incomplete formation of ZnAl₄-LDH was obtained, as evidenced by unreacted bayerite in the PXRD and ^{27}Al NMR spectra, c.f., Table S1 and Figure 2. Three out of the 13 samples, all prepared at 120 °C with a reaction time of one week or longer, are pure based on the Zn:Al ratio from ICP-OES, PXRD, and ^{27}Al SSNMR. The sample ZnAl₄-120-9x2.8 was chosen for extensive structural characterization, it will be referred to as ZnAl₄-LDH in the following except that the TEM data are of the ZnAl₄-120-11x2.8 sample.

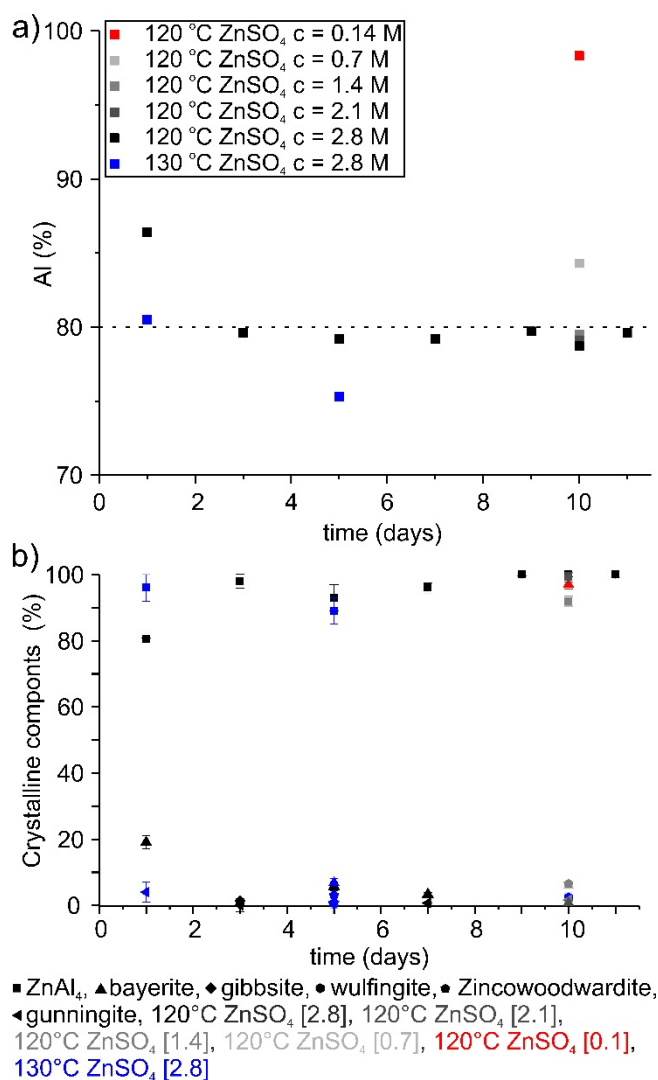


Figure 2. a) The aluminum content (mole%, ICP-OES) as a function of reaction time. The dotted line indicates the Al content in a stoichiometric ZnAl₄-LDH. b) The relative amount of ZnAl₄-LDH, ZnSO₄, and bayerite in the crystalline phases determined by PXRD.

Bulk characterization of the ZnAl₄-LDH:

PXRD diffractogram of ZnAl-nickelalumite² with various Zn concentrations was simulated to probe the effect of Zn substitution on the Al sites, Al was partially replaced by Zn in a static (non-relaxed) model, with Zn occupancies of 0, 0.0625, 0.125, 0.25, 0.5, and 1.0 in these simulated PXRD diffractograms (Figure S2). These simulations were then graphically compared to the simulated

structure of nickelalumite, the $\text{ZnAl}_4\text{-LDH}$ structure by Britto and Kamath,⁸ and the PXRD of the $\text{ZnAl}_4\text{-LDH}$. The PXRD matched our earlier reported data¹¹ and did not contain reflections which could be assigned to the reaction materials or likely impurities, i.e., bayerite, boehmite, gunningite ($\text{ZnSO}_4\cdot\text{H}_2\text{O}$), or a hydrotalcite-like ZnAl-LDH , c.f., Figures 3 and S1. Moreover, the comparison of the experimental and simulated diffractograms did not give indication of Zn substitution on the Al sites. Rietveld refinement provided the following unit cell parameters: space group $\text{P2}_1/\text{n}$, $a = 10.29487(65)$, $b = 8.91160(53)$, $c = 17.14261(77)$, and $\beta = 95.6756(58)$.

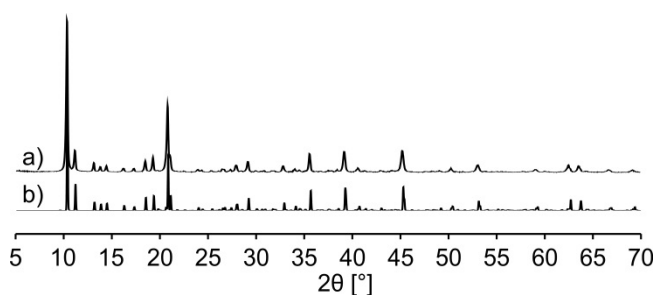


Figure 3. a) The experimental and b) simulated PXRD diffractogram of $\text{ZnAl}_4\text{-LDH}$. The simulation is based on the crystal structure of nickelalumite.²

The Al content is 79.7(5) mole% based on ICP-OES, which is in excellent agreement with theoretical value of 80 % ($\text{Zn}:\text{Al} = 1:4$) within the experimental uncertainties. TEM showed quite thin, rectangular aggregated platelets with a size ranging from ca 300 nm to 3-4 μm , as illustrated in Figure S3. The particle border is well-defined. Furthermore, the thin needles characteristic for boehmite,¹¹ are not observed. In comparison with the particle morphology in our earlier study (100-500 nm thin ill-defined, aggregated platelets)¹¹, the particle size is significantly larger and the morphology more defined, which is ascribed to the extended reaction time (nine vs two days), in agreement with the proposed dissolution reprecipitation mechanism and Ostwald ripening.⁸ The platelets remain thin, but their thickness cannot be determined due to preferred orientation parallel to the grid.

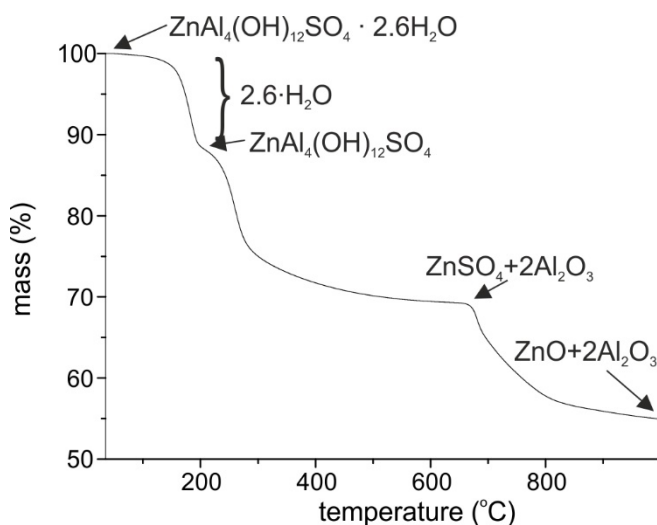
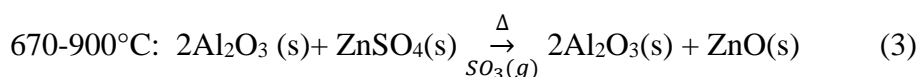
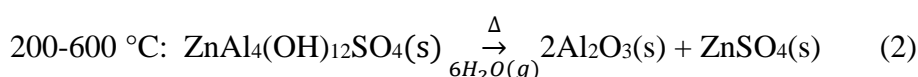
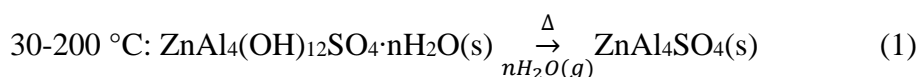


Figure 4. TGA of ZnAl₄-120-9x2.8 (ZnAl₄-LDH) showing the three distinct mass losses.

Thermal analysis by TGA showed three distinct mass losses corresponding to the three reaction below (Eqs. 1-3).⁸



The thermal events (Figure 4, Table S2, and Eqs. 1-3¹⁷) corresponds to 2.62(5) H₂O, 5.99(5) OH, and 0.99(5) SO₄ respectively based on a composition of ZnO + 2 Al₂O₃ for the end product. Thus, a formula of ZnAl₄(OH)_{5.99(5)}(SO₄)·2.62(5) H₂O is derived, i.e., a stoichiometric sample within the experimental uncertainty. The interlayer water content in our sample is ca 10 % lower than the three crystallographic water molecules in nickelalumite.² However, the Cu analogue, chalcoalumite, has a

water content of 3-3.3 interlayer water molecules and positional disorder for one of the interlayer O site from single crystal XRD,¹⁵ i.e., a variable interlayer water content. A variable amount of interlayer water is commonly observed in LiAl-LDH, hydrotalcite-like LDH, and clays. Moreover, changes in the chemical shift region for water layer molecules were observed in the ¹H MAS NMR spectra recorded with ultrafast MAS without cooling (not shown). Thus, the interlayer water content is quite sensitive to the sample temperature and humidity. However, the bulk characterization techniques (PXRD, ICP-OES, TGA) all point to a stoichiometric, pure ZnAl₄-LDH with a well-defined crystal morphology.

Zinc(II) local structural environment from K Edge EXAFS spectroscopy

The full Zn K-edge EXAFS spectrum was fit using the nickelalumite structure,² where the crystallographic M(II) position is fully occupied by Zn, and considered only scattering within the cation layer (Figure 5). The layers are too far apart to have a strong impact on the EXAFS spectrum, and anions between the layers are too disordered with respect to their location. The fits yield a very good R-factor of 0.012, because the number of independent points (N_{ind}) exceed the number of variables (N_{var}) by far (see Table 1 and Figure 5). All variables are within reasonable boundaries, although some distant oxygen atoms shift by up to 0.2 Å, a relatively large (but still acceptable) shift for EXAFS. A relatively prominent feature is seen at 5.6 Å (uncorrected for phase shift), which fits to the Zn–Al oscillations. The low but reasonable σ^2 for these scattering-paths indicates six well-ordered Al at a distance of 6.04 Å (corrected for phase shift) from Zn. The first coordination sphere in ZnAl₄-LDH, which contains two and four oxygen at 1.977(4) and 2.093(2) Å, respectively is significantly different from the first coordinations sphere in hydrotalcite LDH (six oxygen all at ca 2.06 Å).^{29, 30}

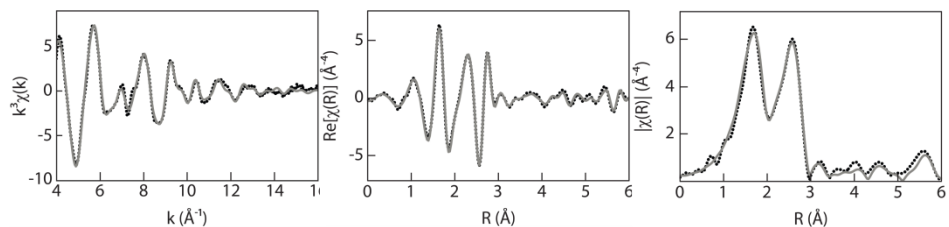


Figure 5. The Zn EXAFS data is showed as the dotted line and the grey line is the simulated data. Normalized k^3 -weighted Zn K -edge spectrum of ZnAl₄-LDH (left), the real part of the Fourier transformed Zn K -edge spectrum (middle) and magnitude of the Fourier transform of the Zn K -edge spectrum. Data for Zn in ZnAl₄-LDH (dotted black line), fit for Zn in ZnAl₄-LDH (solid grey line). All spectra are uncorrected for phase shift.

Table 1. Zn-X distances (X = Al, O, and Zn) determined from analysis of the EXAFS data. The reported single crystal structure of nickelalumite was used as a starting point in the analysis.^{2, 11}

Paths	N	d (Å)	σ^2
Zn-O	2	1.977(4)	0.007
	4	2.093(2)	0.007
	2	3.220(13)	0.008
	2	3.428(16)	0.008
	4	4.613(15)	0.007
	4	4.820(19)	0.007
Zn-Al	3	3.009(4)	0.008
	2	3.021(2)	0.008
	1	3.032 (2)	0.008
	6	6.043(8)	0.005
Zn-Zn	2	5.192(2)	0.012
Zn-O- O-Zn	30	3.680(5)	0.014
$\Delta E_0=0.33$, $N_{\text{var}}=14$, $N_{\text{ind}}=37.81$, $R=0.012$, k-range=4-16, R-range=1-6			

²⁷Al MAS and 3QMAS NMR

The two possible Al containing impurities, bayerite and boehmite are most readily identified and quantified in ²⁷Al MAS and 3QMAS NMR spectra combined with deconvolution of the ²⁷Al single pulse MAS NMR spectra. The presence of bayerite (two ²⁷Al sites with $\delta_{\text{iso}}(^{27}\text{Al}) = 13.3(6)$ and $8.7(4)$ ppm³¹) is most readily seen as a shoulder on the left side of the resonance of single pulse spectra, whereas the single resonance from boehmite ($\delta_{\text{iso}}(^{27}\text{Al}) = 11.7(4)$ ppm³¹) overlap with the ZnAl₄-LDH resonances. Boehmite is best resolved in the 3QMAS NMR spectra recorded at the two moderate magnetic fields (11.7 and 14.1 T) used in our study. The ²⁷Al NMR spectra were analyzed

using our previously reported ^{27}Al NMR parameters¹¹ and literature values³¹ for boehmite and bayerite as starting values.

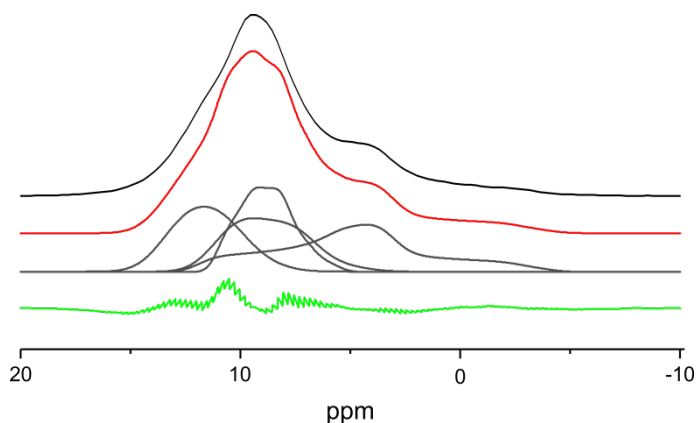


Figure 6. Single pulse ^{27}Al MAS NMR spectrum (black) and the deconvolution of the spectra, where the total spectrum and individual sites are shown in red and black, respectively, using the parameters in Table 2 (14.1 T and 15 kHz spinning).

The ^{27}Al 3QMAS (Figure S4) allowed for identification of the four Al sites as well as estimates of the isotropic chemical shifts and second order quadrupole effect parameters (SOQE). These were used as starting points for simulations of the ^{27}Al MAS NMR spectrum in Figure 6. The results are summarized in Table 2, which are in good agreement with our earlier reported data.¹¹ We note that substantial overlap is seen between Al2 and Al3 due to similar isotropic shifts and size of their quadrupole interaction. No other resonances, in particular bayerite or boehmite could be identified in these ^{27}Al SSNMR spectra of $\text{ZnAl}_4\text{-LDH}$. Thus, from ^{27}Al MAS NMR the sample does not contain Al impurities above the detection limit of ^{27}Al MAS NMR (<5%).

Table 2. ^{27}Al NMR parameters obtained from deconvolution of ^{27}Al MAS NMR spectrum in Figure 6.

ZnAl ₄ -SO ₄ (sites)	$\delta_{\text{iso}}(^{27}\text{Al})$, ppm	C_Q , MHz	η	I (%)
A11	8.2(4)	3.0(3)	0.6	25(4)
A12	11.0(6)	3.1(3)	0.5	24(4)
A13	9.0(6)	3.5(2)	0.3	24(4)
A14	9.0(4)	4.9(2)	0.9	27(5)

Analysis of the ^1H MAS NMR spectra

The nickelalumite structure,² which is isostructural to ZnAl₄-LDH, contains 18 crystallographic inequivalent H sites of which 12 and 6 originate from the –OH and interlayer water, respectively. Our sample contains ca 2.6 water molecules per formula unit according to TGA (*vide supra*). The ^1H MAS SSNMR is therefore expected to contain 12 sites from the ZnAl₄-LDHs structure with one to six resonances from the water depending on the mobility of the water, i.e., a total of 13 to 18 ^1H resonances. 12 different ^1H resonances are unambiguously determined from deconvolution of the ^1H MAS SSNMR spectrum, c.f., Figure S5 and Table 3 with relative intensities spanning from 0.7(4) to 2.7(6) corresponding to a total of 18(2) resonances in agreement with the chemical composition. Even though not all sites are resolved in the spectra, it is still a significant improvement compared to ^1H MAS NMR data at 950 MHz using 35 kHz spinning previously published,¹¹ which showed only seven broad resonances overlapping due to a combination of ca 30 % impurities (bayerite and boehmite) and lower MAS rates.

Table 3. $\delta_{\text{iso}}(^1\text{H})$ and relative concentration of the different ^1H resonances obtained from deconvolution of the ^1H MAS NMR spectrum in Figure S5. The relative intensity (I) and the corresponding number of the protons (#H) is given. Only the isotropic resonance was included in the deconvolution. The structure contains 18 crystallographic inequivalent ^1H .² One hydrogen corresponds to 6 % of the total intensity.

$\delta_{\text{iso}}(^1\text{H})$ (ppm)	I (%)	#H
1.9(17)	6(5)	1
2.7(7)	4(4)	1
3.2(6)	8(3)	1
3.8(6)	8(3)	1
4.4(8)	12(5)	2
4.8(7)	4(3)	1
5.2(7)	11(4)	2
5.9(8)	16(5)	3
6.5(6)	10(4)	2
7.2(6)	11(3)	2
7.7(7)	4(2)	1
8.3(5)	6(3)	1
Total		18

First, the ^1H NMR resonances from the interlayer water molecules were identified by measurement of the T_2' by a series of spin-echo experiments with different echo spacing. The three ^1H resonances

at $\delta_{\text{iso}}(^1\text{H}) = 4.4, 5.2, \text{ and } 5.9$ ppm have the shortest T_2' (Table S3) and weaker intensity in the ^1H - ^1H correlation NMR experiment (*vide infra*). The observation of several resonances from the interlayer water implies limited mobility on the NMR time scale. This is in strong contrast to the single resonance seen for the highly mobile (disordered) interlayer water in hydrotalcite-like LDH such as MgAl, ZnAl, MgGa, and NiAl-LDH.³²⁻³⁵

^{27}Al - ^1H correlations from ^1H , ^{27}Al D-HMQC NMR

Figure 1b shows the local Al and H coordination network in the cation layer. Standard ^1H , ^{27}Al D-HMQC MAS NMR spectra showed substantial overlap of the Al resonances, which prevented a detailed analysis, not surprising given the significant overlap in the ^{27}Al MAS NMR spectrum (Figure 6). Simulations using the ^{27}Al NMR parameters for ZnAl₄-LDH (Table 2) revealed that the satellite transitions from the Al₄ site are separated from the main resonances in a ^{27}Al , ^1H HMQC spectrum at 14.1 T due to a significantly larger second order quadrupole shift (Figure S6). Thus, a ^1H , ^{27}Al D-HMQC MAS NMR spectrum recorded with rotor-synchronization the spinning side bands from the Al₄ sites folded on to the isotropic resonance for the outermost satellite transition (Figure 7). Slices from the 2D ^1H , ^{27}Al D-HMQC MAS NMR spectrum in the region for the Al₄ satellite transitions showed that Al₄ is coordinated to the six protons with $\delta(^1\text{H}) = 3.0, 3.4, 4.5, 6.4, 7.1, \text{ and } 8.3$ ppm. Furthermore, the resonances at $\delta(^1\text{H}) = 2.7, 3.8, 5.9, 7.2, \text{ and } (7.3/7.7)$ ppm are correlated to Al₂, which has the highest isotropic shift, was extracted from a non-rotor synchronized ^1H , ^{27}Al HETCOR spectrum at 22.3 T (not shown). This served as a starting point for the assignment of the remaining proton resonances, which was obtained by analysis of ^1H , ^1H NOESY NMR spectra (Figures 7 and S5). Table 4 summarizes the assignment of the ^1H and ^{27}Al resonances, whereas further details are given in the supporting information (Tables S4-S6).

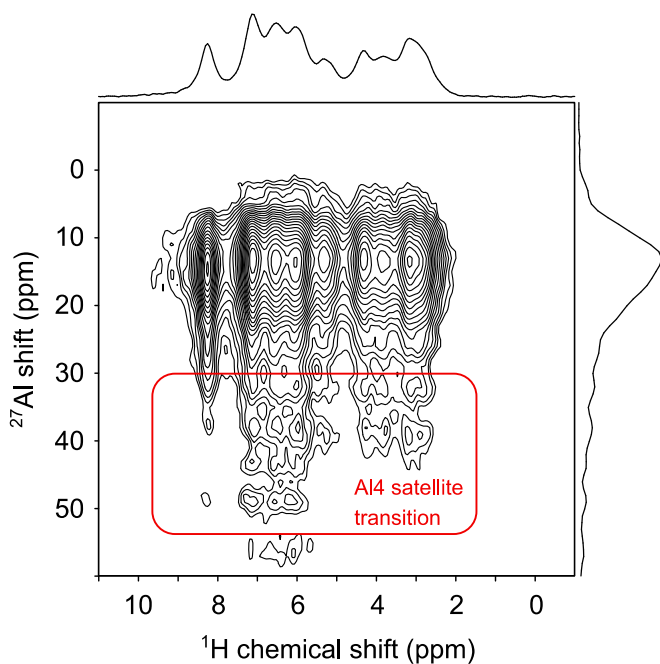


Figure 7. ^1H , ^{27}Al D-HMQC with rotor synchronization illustrating the separation of the satellite transitions from the Al4 resonances, which allowed unambiguous assignment of the six -OH groups coordinated to Al4. The spectrum was recorded at 14.1 T using 80 kHz spinning.

From the crystal structure of nickelalumite it is known that H9, H10, H12, H15, H17, and H18 are coordinated to Al4, whereas H7, H9, H13, H16, and H17 are coordinated to Al2, c.f., Table S4. Only the two ^1H resonances at 2.7 and 7.2 ppm are correlated to both Al2 and Al4. The only two hydrogen coordinated to both in the crystal structure are H9 and H17, which are $\text{ZnAl}_2\text{-OH}$ and $\text{Al}_2\text{-}$

Table 4. ^1H and ^{27}Al correlations from analysis of the spectra in Figures 7-10 and S4-S7 with tentative assignment based on the NMR data. The intensity is from Table 3.

^1H (δ_{iso} (ppm))	site	Correlated ^1H	Correlated ^{27}Al	Assignment	Int
1.9(2)		1.9	none	impurity	1
2.7(7)		4.8	Al1/Al3, Al2	H17	1
3.2(6)		3.8, 5.2, 5.9, 8.3	Al1/Al3, Al4	H12	1
3.8(6)		4.8 7.1	Al1/Al3	H16	1
4.4(8)			Al1/Al3, Al4	H18 + water	2
4.8(7)		3.5, 5.9, 7.2, 8.3	Al1/Al3	H11	1
5.2(7)		3.5		water	2
5.9(8)		2.7, 5.2, 7.2, 8.3	Al1/Al3, Al2	H7 + water	3
6.5(6)		3.5, 7.2	Al/Al3, Al4	H15 + H8 or H14	2
7.2(6)		1.9, 3.5, 8.3	Al1/Al3, Al2, Al4	H9 + H8 or H14	2
7.7(7)			Al1/Al3 and Al2	H13	1
8.3(5)		4.8, 5.9 and 7.2	Al2, and Al4	H10	1

OH groups, respectively. There are two types of hydroxyl groups in ZnAl_4 : $\text{Al}_2\text{-OH}$ and $\text{ZnAl}_2\text{-OH}$ (six crystallographic inequivalent of each). Bayerite contains three ^1H resonances at 3.0, 4.3, and 5.0 ppm from $\text{Al}_2\text{-OH}$.³¹ $\text{ZnAl}_2\text{-OH}$ are observed in defect hydrotalcite ZnAl-LDH at $\delta(^1\text{H}) > 4.6$ ppm¹¹ and similarly $\text{MgAl}_2\text{-OH}$ groups in MgAl-LDH .³⁶ Furthermore, the ^1H shifts obtained from DFT calculations¹¹ systematically show the $\text{ZnAl}_2\text{-OH}$ groups to have the highest shifts further. Thus, we assign the two protons coordinated to both Al2 and Al4 located 2.7 and 7.2 ppm to H17 ($\text{Al}_2\text{-OH}$) and H9 ($\text{ZnAl}_2\text{-OH}$), respectively.

Based on the assumption that the $\text{Al}_2\text{-OH}$ groups have a lower chemical shift than $\text{ZnAl}_2\text{-OH}$ the ^1H resonance at 3.8 ppm corresponds to H16 as it is the only other $\text{Al}_2\text{-OH}$ group coordinated the Al2. Similarly, the resonance at 8.3 ppm is assigned to H10 as it is the only other $\text{ZnAl}_2\text{-OH}$ group coordinated to Al4. The ^1H resonance at 4.8 ppm, which is correlated to Al1 and/or Al3 but neither Al2 nor Al4, is assigned to H11 as the isotropic shift similar to bayerite. H11 is the only $\text{Al}_2\text{-OH}$

group which is not coordinated to Al2 and Al4. Thus, five out of twelve -OH groups have been assigned.

¹H-¹H correlations from ¹H,¹H NOESY NMR Spectra

The ¹H-¹H correlations observed in ¹H,¹H NOESY spectra (Figures 8 and S7) are now used to further improve the assignment. The ¹H resonances at 5.9 and 7.7 ppm belongs to H7 and H13, based on the correlation to Al2 and high $\delta(^1\text{H})$. A correlation between the $\delta(^1\text{H}) = 5.9$ ppm and 8.3 ppm (H10) resonances is observed in the NOESY spectrum at short contact times (1 ms, Figure 7), whereas no correlations is seen between the $\delta(^1\text{H}) = 7.7$ and 8.3 ppm (H17). The ¹H resonances at 5.9 ppm and 7.7 ppm are assigned to H7 and H10, respectively, as their distance to H17 is 2.7 (H7) and 4.8 (H13) Å respectively.

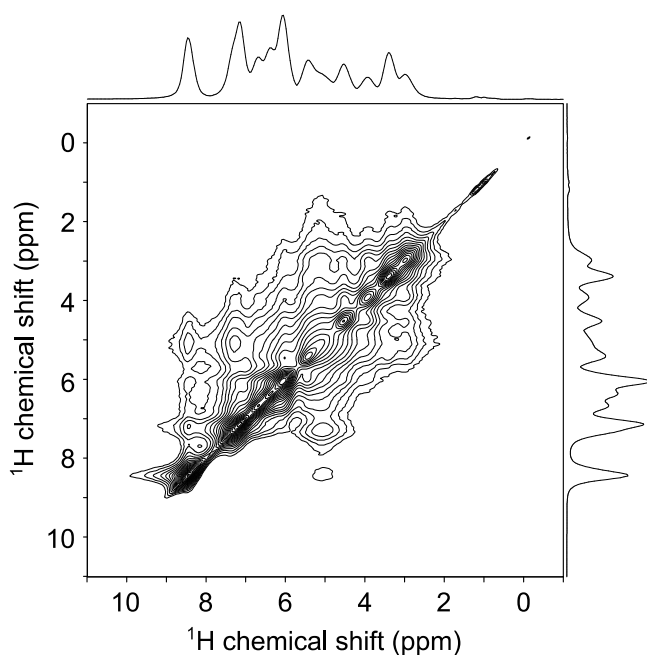


Figure 8. ¹H,¹H NOESY NMR spectrum recorded at $B_0 = 21.1$ T with a spinning speed of 80 kHz.

The mixing time was set to 1 ms to only probe ¹H in close spatial proximity.

The ^1H resonances at 3.2, 4.4, and 6.5 ppm are from H12, H15, and H18 based on the correlations to Al4 observed in the ^1H , ^{27}Al - *D*-HMQC. Only the ^1H resonance at 4.4 ppm is correlated with the H17 resonance at 2.7 ppm in the ^1H , ^1H NOESY with a short mixing time (Figure 8). The distance from H17 to H12, H15, and H18 are 3.1 Å, 4.9 Å, and 2.5 Å, respectively. Thus, the 4.4 ppm resonance is assigned to H18, which has the shortest distance.

^1H - ^1H correlations between the resonances at 3.2 ppm and 3.9 ppm (H16) is observed in NOESY (1 ms), the distance between H12-H16 and H15-H16 in the nickelalumite structure is 3.1 and 4.9 Å, respectively. The ^1H signal at 3.2 ppm is therefore assigned as H12, which means that the ^1H signal at 6.5 ppm can be assigned to H15.

The ^1H signals at 4.4, 5.2, and 5.9 ppm are assigned to water based on the loss of intensity observed in ^1H , ^{27}Al *D*-HMQC and ^1H Hahn echo NMR spectra. Thus, two resonances at 6.5 and 7.2 ppm, which have not been assigned, must belong to H8 and H14, which are both from $\text{ZnAl}_2\text{-OH}$ groups (Table S4), but unambiguous assignment is not possible due to spectral overlap. To conclude, it was possible to assign sixteen of the eighteen crystallographic inequivalent H based on SSNMR.

Conclusions:

Several pure $\text{ZnAl}_4\text{-LDH}$ were obtained after extensive synthesis optimization, which clearly showed that hydrothermal treatment of the sample at moderate temperatures (120 °C) and a reaction time of 9-11 days favor the formation of a pure, crystalline product. This contrasts the previous results in literature, which have employed just one to two day of reaction time at 150-160 °C.^{7, 9, 10, 13, 14, 17} Moreover, the extended reaction time increases the average crystallinity and particle size according to TEM, as compared to our recent study.¹¹ In addition, the excess amount of Zn salt needed could be reduced by 50 % and still yielded a pure sample. A pure sample with a chemical

composition of $\text{ZnAl}_4(\text{OH})_{12}(\text{SO}_4)\cdot 2.6 \text{ H}_2\text{O}$, which was prepared by hydrothermal treatment for nine days at 120 °C, was subject to a detailed structural characterization. The sample composition was determined based on TGA and ICP-OES. Simulation of the PXRD diffractograms and EXAFS unambiguously confirmed that Zn does not substitute on any of the four crystallographic Al sites. Similarly, the ^1H MAS single pulse as well as ^{27}Al single pulse and 3QMAS NMR spectra confirmed the sample purity.

Nearly all ^1H and ^{27}Al NMR resonances could be assigned to using ^1H , ^{27}Al HMQC and ^1H , ^1H NOESY spectra recorded at an ultra-high magnetic field using very fast MAS. The interlayer water molecules were shown to be inequivalent on the NMR time scale in contrast to the high mobility seen in the hydrotalcite-like LDHs. Moreover, a much larger variation in the ^1H chemical shift implying that the acid-base properties of the hydroxyl groups are quite different from the basic -OH groups in hydrotalcite-like LDH. Thus, our results provide a detailed protocol for synthesis optimization and a protocol for reliable structural characterization thereby facilitating the possibility to link the chemical properties of $\text{MAl}_4\text{-LDH}$ to their atomic level structure.

Supporting information available:

Synthesis conditions used for the optimization PXRD of all samples, simulated PXRD as a function of Zn substitution on the Al site, mass loss from TGA, TEM of $\text{ZnAl}_4\text{-120-11x2.8}$, ^{27}Al 3QMAS NMR, ^1H MAS NMR spectrum of $\text{ZnAl}_4\text{-LDH}$, T_2' (^1H), simulated ^{27}Al MAS NMR spectrum, and ^1H - ^1H NOESY spectrum (5 ms) as well as ^1H and ^{27}Al bonding network and ^1H NMR shifts from DFT calculations.

Acknowledgements:

Professor Claude Forano is thanked for valuable discussions. The authors are grateful for financial support from a "Villum Young Investigator Programme" (VKR022364; UGN, NDJ, CAR), The Villum Center for Bioanalytical Services (600 MHz NMR), and Innovationsfonden (ReCoverP). YN and UGN would like to acknowledge JSPS fellowship ID no: S18054 from The Japanese Society for Promotion of Sciences. Ms Carina Lohman is thanked for performing the ICP-OES measurements. The Danish Research Council for Science and Nature (Dancatt) is thanked for financial support related to the EXAFS experiments. The 950 MHz NMR spectra were recorded at the Danish Center for Ultrahigh-Field NMR spectroscopy, Århus (Ministry of Higher Education and Science, grants AU-2010-612-181).

References:

1. Duan, X.; Evans, D. G., *Layered Double Hydroxides*. 2006, Springer
2. Uvarova, Y. A.; Sokolova, E.; Hawthorne, F. C.; Karpenko, V. V.; Agakhanov, A. A.; Pautov, L. A., The crystal chemistry of the "nickelalumite"-group minerals. *Can Miner.* **2005**, *43*, 1511-1519.
3. Besserguenev, A. V.; Fogg, A. M.; Francis, R. J.; Price, S. J.; O'Hare, D.; Isupov, V. P.; Tolochko, B. P., synthesis and structure of the gibbsite intercalation compounds $[\text{LiAl}_2(\text{OH})_6]\text{X}$ {X=Cl, Br, NO_3 } and $[\text{LiAl}_2(\text{OH})_6]\text{Cl} \cdot \text{H}_2\text{O}$ using synchrotron X-ray and neutron powder diffraction. *Chem Mater.* **1997**, *9*, 241-247.
4. Fogg, A. M.; Dunn, J. S.; Shyu, S. G.; Cary, D. R.; O'Hare, D., Selective ion-exchange intercalation of isomeric dicarboxylate anions into the layered double hydroxide $[\text{LiAl}_2(\text{OH})_6]\text{Cl} \cdot \text{H}_2\text{O}$. *Chem. Mater.* **1998**, *10*, 351-355..

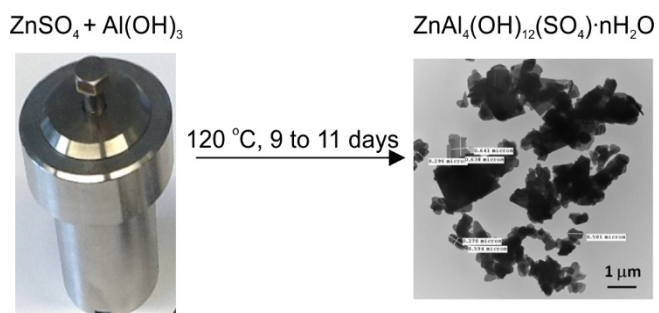
5. Hou, X.; Kalinichev, A. G.; Kirkpatrick, R. J., Interlayer Structure and Dynamics of Cl–LiAl₂-Layered Double Hydroxides: ³⁵Cl NMR Observations and Molecular Dynamics Modelling. *Chem. Mater.* **2002**, *14*, 2078.
6. Nagendran, S.; Periyasamy, G.; Kamath, P. V., Structure models for the hydrated and dehydrated nitrate-intercalated layered double hydroxide of Li and Al. *Dalton Trans.* **2016**, *45*, 18324-18332.
7. Britto, S.; Kamath, P. V., Structure of Bayerite-Based Lithium-Aluminum Layered Double Hydroxides (LDHs): Observation of Monoclinic Symmetry. *Inorg. Chem.* **2009**, *48*, 11646-11654.
8. Britto, S.; Kamath, P. V., Polytypism, Disorder, and Anion Exchange Properties of Divalent Ion (Zn, Co) Containing Bayerite-Derived Layered Double Hydroxides. *Inorg. Chem.* **2010**, *49*, 11370-11377.
9. Chitrakar, R.; Makita, Y.; Sonoda, A.; Hirotsu, T., Synthesis of a novel layered double hydroxides [MgAl₄(OH)₁₂]Cl₂ · 2.4H₂O and its anion-exchange properties. *J Hazard Mater.* **2011**, *185*, 1435-1439.
10. Fogg, A. M.; Williams, G. R.; Chester, R.; O'Hare, D., A novel family of layered double hydroxides - [MAl₄(OH)₁₂](NO₃)₂ · H₂O (M = Co, Ni, Cu, Zn). *J. Mater Chem.* **2004**, *14*, 2369-2371.
11. Pushparaj, S. S. C.; Jensen, N. D.; Forano, C.; Rees, G. J.; Prevot, V.; Hanna, J. V.; Ravnsbæk, D. B.; Bjerring, M.; Nielsen, U. G., Structural Investigation of Zn(II) Insertion in Bayerite, an Aluminum Hydroxide. *Inorg. Chem.* **2016**, *55*, 9306-9315.
12. Rees, J. R.; Burden, C. S.; Fogg, A. M., New layered double hydroxides by prepared by the intercalation of gibbsite. *J Solid State Chem.* **2015**, *224*, 36-39.

13. Williams, G. R.; Dunbar, T. G.; Beer, A. J.; Fogg, A. M.; O'Hare, D., Intercalation chemistry of the novel layered double hydroxides $[\text{MAl}_4(\text{OH})_{12}](\text{NO}_3)_2 \cdot \gamma \cdot \text{H}_2\text{O}$ (M = Zn, Cu, Ni and Co).. 1: New organic intercalates and reaction mechanisms. *J. Mater. Chem.* **2006**, *16*, 1222-1230.
14. Williams, G. R.; Moorhouse, S. J.; Prior, T. J.; Fogg, A. M.; Rees, N. H.; O'Hare, D., New insights into the intercalation chemistry of $\text{Al}(\text{OH})_3$. *Dalton Trans.* **2011**, *40*, 6012-6022.
15. Hawthorne, F. C.; Cooper, M. A., The crystal structure of chalcoalumite: mechanisms of Jahn-Teller-driven distortion in $[\text{6}]\text{Cu}^{2+}$ -containing oxysalts. *Miner. Mag.* **2013**, *77*, 2901-2912.
16. Williams, G. R.; Dunbar, T. G.; Beer, A. J.; Fogg, A. M.; O'Hare, D., Intercalation chemistry of the novel layered double hydroxides $[\text{MAl}_4(\text{OH})_{12}](\text{NO}_3)_2 \cdot \gamma \cdot \text{H}_2\text{O}$ (M = Zn, Cu, Ni and Co). 2: Selective intercalation chemistry. *J. Mater. Chem.* **2006**, *16*, 1231-1237.
17. Britto, S.; Kamath, P. V., Synthesis, structure refinement and chromate sorption characteristics of an Al-rich bayerite-based layered double hydroxide. *J Solid State Chem.* **2014**, *215*, 206-210.
18. Poeppelmeier, K. R.; Hwu, S. J., Synthesis of Lithium Dialuminate by Salt Imbibition. *Inorg. Chem.* **1987**, *26*, 3297-3302.
19. Döbelin, N.; Kleeberg, R., Profex: a graphical user interface for the Rietveld refinement program BGMN. *J Appl. Crystallogr.* **2015**, *48*, 1573-1580.
20. Klementiev, K. V. www.cells.es/Beamlines/CLAESS/software/xafsmass.html (accessed November 14th, 2018).

21. Ravel, B.; Newville, M., ATHENA, ARTEMIS, HEPHAESTUS: data analysis for X-ray absorption spectroscopy using IFEFFIT. *J. Synchrotron Radiation* **2005**, *12*, 537-541.
22. Mustre de Leon, J.; Rehr, J. J.; Zabinsky, S. I.; Albers, R. C., Ab initio curved-wave x-ray-absorption fine structure. *Phys. Rev. B* **1991**, *44*, 4146-4156.
23. Amoureux, J. P.; Fernandez, C., Triple, quintuple and higher order multiple quantum MAS NMR of quadrupolar nuclei. *Solid State Nucl. Magn.* **1998**, *10*, 211-223.
24. Cavadini, S.; Abraham, A.; Bodenhausen, G., Proton-detected nitrogen-14 NMR by recoupling of heteronuclear dipolar interactions using symmetry-based sequences. *Chem. Phys. Lett.* **2007**, *445*, 1-5.
25. Gan, Z., ¹³C/¹⁴N heteronuclear multiple-quantum correlation with rotary resonance and REDOR dipolar recoupling. *J. Magn. Reson.* **2007**, *184*, 39-43.
26. Gan, Z.; Amoureux, J. P.; Trébosc, J., Proton-detected ¹⁴N MAS NMR using homonuclear decoupled rotary resonance. *Chem. Phys. Lett.* **2007**, *435*, 163-169.
27. Brinkmann, A.; Kentgens, A. P. M., Proton-Selective ¹⁷O–H Distance Measurements in Fast Magic-Angle-Spinning Solid-State NMR Spectroscopy for the Determination of Hydrogen Bond Lengths. *J. Am. Chem. Soc.* **2006**, *128*, 14758-14759.
28. Kemp, T. F.; Smith, M. E., QuadFit--a new cross-platform computer program for simulation of NMR line shapes from solids with distributions of interaction parameters. *Solid State Nucl. Magn. Reson.* **2009**, *35*, 243-52.
29. d'Espinose de la Caillerie, J.-B.; Kermarec, M.; Clause, O., Impregnation of .gamma.-Alumina with Ni(II) or Co(II) Ions at Neutral pH: Hydrotalcite-Type Coprecipitate Formation and Characterization. *J. Am. Chem. Soc.* **1995**, *117*, 11471-11481.

30. Li, W.; Livi, K. J.; Xu, W.; Siebecker, M. G.; Wang, Y.; Phillips, B. L.; Sparks, D. L., Formation of crystalline Zn-Al layered double hydroxide precipitates on gamma-alumina: the role of mineral dissolution. *Environ. Sci. Technol.* **2012**, *46*, 11670-7.
31. Damodaran, K.; Rajamohanan, P. R.; Chakrabarty, D.; Racherla, U. S.; Manohar, V.; Fernandez, C.; Amoureux, J.-P.; Ganapathy, S., Triple-Quantum Magic Angle Spinning ^{27}Al NMR of Aluminum Hydroxides. *J. Am. Chem. Soc.*, **2002**; *124*, 3200-3201.
32. Pushparaj, S. S. C.; Forano, C.; Prevot, V.; Lipton, A. S.; Rees, G. J.; Hanna, J. V.; Nielsen, U. G., How the Method of Synthesis Governs the Local and Global Structure of Zinc Aluminum Layered Double Hydroxides. *J. Phys. Chem. C* **2015**, *119*, 27695-27707.
33. Sideris, P. J.; Nielsen, U. G.; Gan, Z. H.; Grey, C. P., Mg/Al ordering in layered double hydroxides revealed by multinuclear NMR spectroscopy. *Science* **2008**, *321* (5885), 113-117.
34. Yu, G.; Hu, F.; Huo, H.; Ding, W.; Peng, L., Probing local structure of paramagnetic Ni-Al layered double hydroxides with solid-state ^2H NMR spectroscopy. *Chem. Phys. Lett.* **2018**, *706*, 47-52.
35. Petersen, L. B.; Lipton, A. S.; Zorin, V.; Nielsen, U. G., Local environment and composition of magnesium gallium layered double hydroxides determined from solid-state ^1H and ^{71}Ga NMR spectroscopy. *J Solid State Chem.* **2014**, *219*, 242-246.
36. Cadars, S.; Layrac, G. r.; Gérardin, C.; Deschamps, M. l.; Yates, J. R.; Tichit, D.; Massiot, D., Identification and Quantification of Defects in the Cation Ordering in Mg/Al Layered Double Hydroxides. *Chem. Mater.* **2011**, *23*, 2821-2831.

For table of contents only



Synopsis

Pure $\text{ZnAl}_4(\text{SO}_4) \cdot n\text{H}_2\text{O}$ was obtained by a reaction of bayerite, $\text{Al}(\text{OH})_3$, and a concentrated $\text{Zn}(\text{II})$ sulfate solution under mild hydrothermal conditions ($120\text{ }^\circ\text{C}$) for nine to eleven days, as evident from extensive synthesis optimization. Structural characterization of $\text{ZnAl}_4(\text{SO}_4) \cdot 2.6\text{H}_2\text{O}$ by PXRD, Zn K-edge EXAFS, TGA, TEM, and solid-state NMR show a highly crystalline material without defects in the cation layer and strongly hydrogen bonded water in the interlayer.

Supporting Information

Synthesis and structural characterization of a pure $\text{ZnAl}_4(\text{OH})_{12}(\text{SO}_4)\cdot 2.6 \text{ H}_2\text{O}$ layered double hydroxide

Nicholai Daugaard Jensen¹, Nghia Tuan Duong², Ralph Bolanz³, Yusuke Nishiyama^{2,4,5}, Camilla Aistrup Rasmussen¹, Jorg Gottlicher⁶, Ralph Steininger⁶, Vanessa Prevot,⁷ and Ulla Gro Nielsen^{1*}

¹ Department of Physics, Chemistry, and Pharmacy, University of Southern Denmark, Campusvej 55, 5230 Odense M, Denmark SDU

² RIKEN-JEOL Collaboration Center, RIKEN, Yokohama, Kanagawa 230-0045, Japan

³ Friedrich-Schiller-University, Institute of Geosciences, Carl-Zeiss-Promenade 10, 07745 Jena, Germany

⁴ NMR Science and Development Division, RIKEN SPring-8 Center, Tsurumi, Yokohama, Kanagawa 230-0045, Japan

⁵ JEOL RESONANCE Inc., Musashino, Akisma, Tokyo 186-8558, Japan

⁶ Karlsruhe Institute of Technology, Institute for Photon Science and Synchrotron Radiation (IPS), Hermann-vn-Helmholtz Platz 1, D-79344 Eggenstein-Leopoldshafen, Germany

⁷ Université Clermont Auvergne, CNRS, SIGMA Clermont, ICCF, F-63000 Clermont-Ferrand, France

	Page
Sample naming convention	S2
Table S1: Synthesis parameters used for optimization experiments	S3
Figure S1: PXRD of samples and reference compounds	S4
Figure S2: The effect of Zn substitution on the PXRD pattern	S5
Table S2: Mass loss in TGA	S6
Figure S3: TEM of ZnAl ₄ -LDH	S6
Figure S4: ²⁷ Al 3QMAS NMR spectrum	S7
Figure S5: Deconvolution of the ¹ H MAS NMR spectrum	S7
Table S3: T ₂ ' determined by ¹ H MAS NMR spin echo experiments	S8
Figure S6: Simulated ²⁷ Al, ¹ H HMQC spectrum	S9
Figure S7: ¹ H, ¹ H NOESY with a mixing time of 5 ms	S10
Table S4: Coordination of the different H sites	S10
Table S5: ¹ H, ²⁷ Al correlation network from SSNMR spectra	S11
Table S6: Calculated ¹ H shifts from DFT	S12
References	S13

Sample naming convention

The sample naming convention is: ZnAl₄-PPP-YxZZ, where PPP, Y, and ZZ indicate the temperature (°C) of the hydrothermal treatment, the duration of hydrothermal treatment (days), and ZZ denotes concentrations of the zinc sulfate solution, respectively.

Table S1. The synthesis conditions including: concentration of the zinc sulfate (c(Zn), autoclave size, temperature (T), and duration (Time) of the hydrothermal treatment. The Al concentration in the solid product (ICP-OES), and the crystalline phases identified by PXRD (Fig. 2a summarizes the quantities). The following abbreviations are used: bayerite (Ba), boehmite (Bo), gibbsite (Gi), gunningite (Gu), wulfingite (Wu), zincowoodwardite ($Zn_{1-x}Al_x$ -LDH, a hydrotalcite ZnAl-LDH), and ZnAl₄-LDH. Samples in bold are pure and stoichiometric according to PXRD, ICP-OES and ²⁷Al SSNMR. S, M and L indicates a concentration of ≤ 5%, 5-25% and above 25%.

Sample	T (°C)	Time (days)	c(Zn). (M)	Autoclave size (mL)	Al (%)	Crystalline phases
ZnAl ₄ -120-1x2.8	120	1	2.8	40	86.4(6)	Ba(M), ZnAl ₄ (L)
ZnAl ₄ -120-3x2.8	120	3	2.8	40	79.6(6)	Gi(S), Gu(S), ZnAl ₄ (S)
ZnAl ₄ -120-5x2.8	120	5	2.8	40	79.2(6)	Ba(S), Gu(S), ZnAl ₄ (L)
ZnAl ₄ -120-7x2.8	120	7	2.8	40	79.2(6)	Ba(S), ZnAl ₄ (L)
ZnAl₄-120-9x2.8	120	9	2.8	40	79.7(6)	ZnAl₄(L)
ZnAl ₄ -120-10x0.1	120	10	0.1	40	98.3(6)	Ba(L), ZnAl ₄ (S)
ZnAl ₄ -120-10x0.7	120	10	0.7	40	84.3(6)	Ba(L), Wu(S), ZnAl ₄ (S)
ZnAl ₄ -120-10x1.4	120	10	1.4	40	79.5(6)	Gu(S), Wu(S), Zn _{1-x} Al _x -LDH(S), ZnAl ₄ (L)
ZnAl ₄ -120-10x2.1	120	10	2.1	40	79.1(6)	Ba(S), ZnAl ₄ (L)
ZnAl₄-120-10x2.8	120	10	2.8	40	78.7(6)	ZnAl₄(L)
ZnAl₄-120-11x2.8	120	11	2.8	40	79.6(6)	ZnAl₄(L)
ZnAl ₄ -130-1x2.8	130	1	2.8	80	80.5(6)	Gu(S), ZnAl ₄ (L)
ZnAl ₄ -130-5x2.8	130	5	2.8	80	75.3(6)	Ba,(S) Bo(S), Gu(S), Wu(S), Zn _{1-x} Al _x -LDH(S), ZnAl ₄ (L)

Bayerite, Al(OH)₃, gibbsite Al(OH)₃, boehmite γ -AlOOH, gunningite: ZnSO₄ · H₂O, wulfingite Zn(OH)₂,

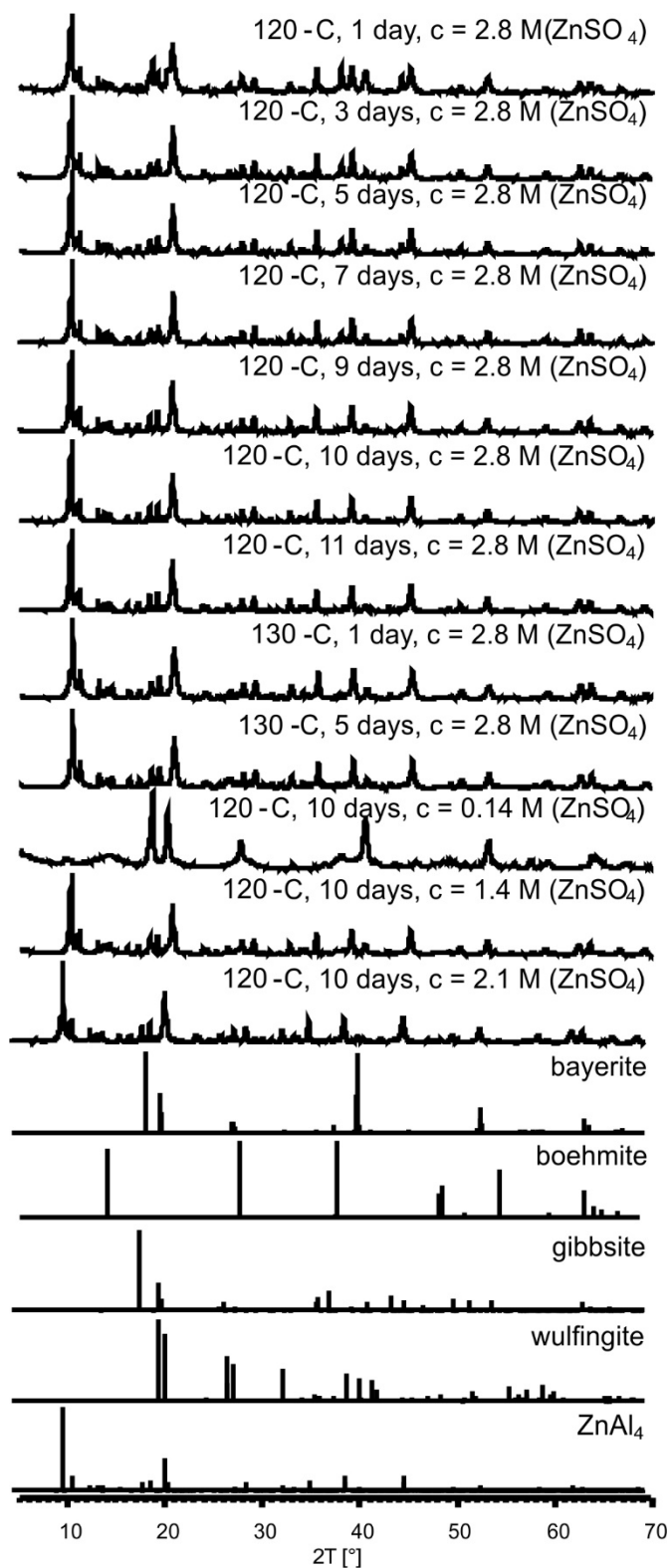


Figure S1. PXRD (Cu K α) of all samples in Table S1 and relevant reference materials.

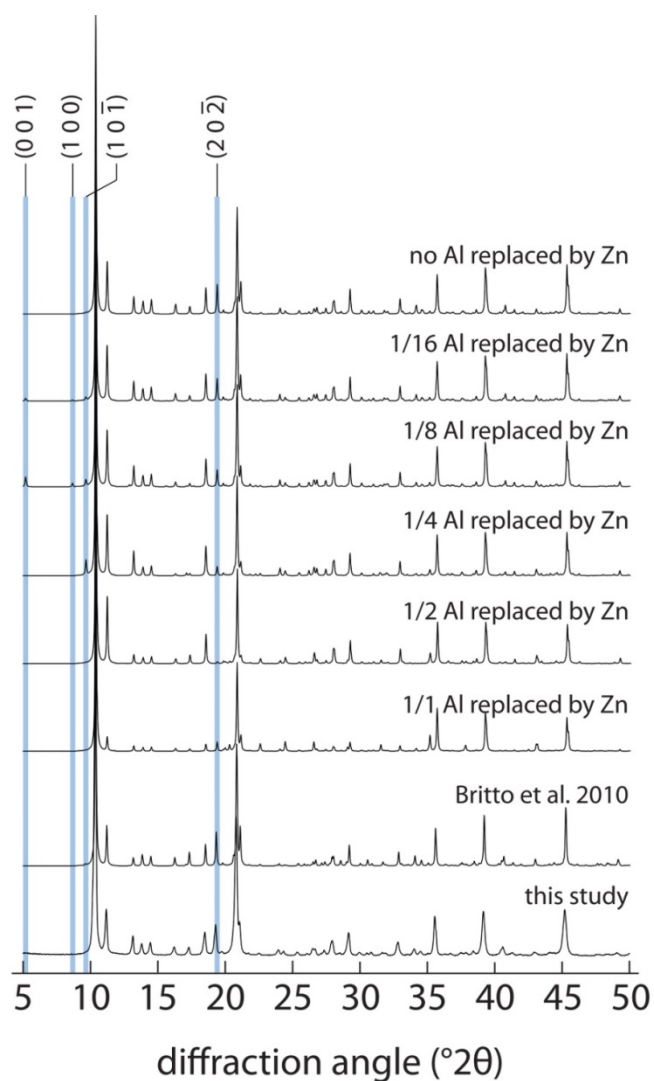


Figure S2. The effect on Zn substitution on the PXR D diffractograms (Cu $K\alpha$ radiation) of $ZnAl_4$ -LDH with the four reflections, that are most affected marked. The single crystal structure of nickelalumite¹ was used as a starting point. The Zn occupancy on the Al1 site varied as indicated in the figure. For a comparison, the PXR D diffractogram calculated using data reported by Britto and Kamanth² (22% Zn substitution on the Al1 site) and the diffractogram of our $ZnAl_4$ -LDH (No Zn substitution). As the Zn occupancy is increased from zero to full occupancy on the Al1 site, the (0 0 1), (1 0 0), and (1 0 -1) increase in intensity, while the (2 0 -2) reflection decreases. The structure published by Britto et al.³ has weak indications of Zn–Zn neighboring in the (1 0 -1) reflection. In contrast, the intensity of the (1 0 -1) reflection stays below the detection limit for our pure $ZnAl_4$ -LDH as expected.

Table S2. Mass losses observed in the TGA in Figure 4.

Temperature	Mass (mg)	Mass loss (mg)	Component loss	Component	Comment
30 °C	16.79			$\text{ZnAl}_4(\text{OH})_{12}\text{SO}_4 \cdot 2.6\text{H}_2\text{O}$	
186 °C	15.27	1.52	2.62 H ₂ O	$\text{ZnAl}_4(\text{OH})_{12}\text{SO}_4$	Loss of interlayer and physisorbed water
497 °C	11.57	3.49	6H ₂ O	$\text{ZnSO}_4 + 2\text{Al}_2\text{O}_3$	Loss of OH groups
995 °C	9.20	2.58	SO ₃	$\text{ZnO} + 2\text{Al}_2\text{O}_3$	Loss of SO ₃

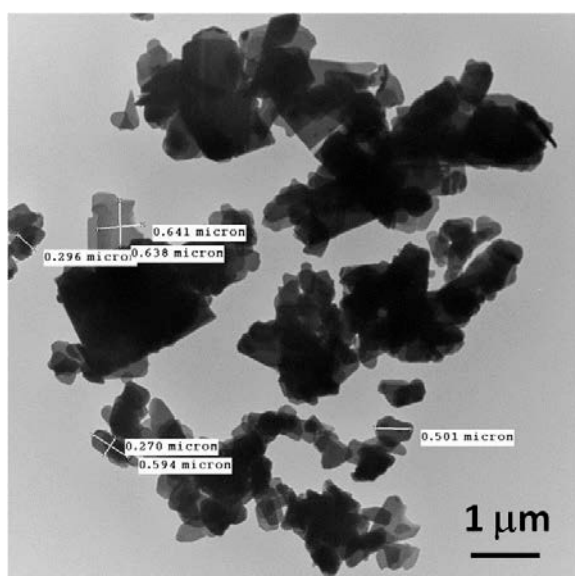


Figure S3. TEM picture of $\text{ZnAl}_4\text{-120-11x2.8}$ with the size of representative crystallites indicated. The thickness of the crystals could not be measured due to preferred orientation, but the particles are significantly thinner than the other two length scales.

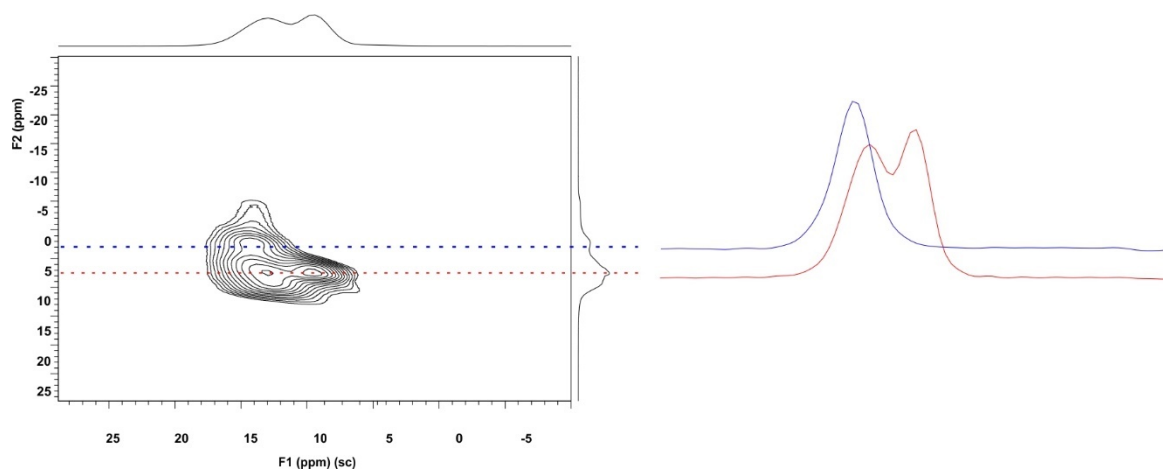


Figure S4: ^{27}Al 3QMAS NMR spectrum of $\text{ZnAl}_4\text{-LDH}$ ($\text{ZnAl}_4\text{-120-9x2.8}$) at 14.1 T using 15 kHz spinning speed

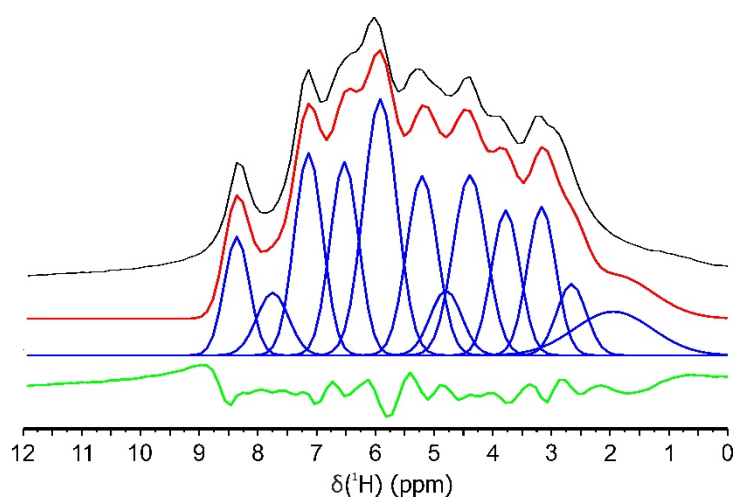


Figure S5. ^1H MAS NMR spectrum and deconvolution using the minimum number of resonances (12) needed to reproduce the overall line width (14.1 T and 80 kHz spinning). The results from the deconvolution are summarized in Table 3.

Table S3. T_2' determined from a series of ^1H spin-echo experiments at 21.1 T, which allowed for identification of the interlayer water resonances at $\delta(^1\text{H})$ of 4.56, 5.09, and 5.37 ppm.

$\delta(^1\text{H})$ (ppm)	T_2' (ms)	χ^2
8.46	3.3	0.0002
7.20	2.4	0.0005
6.68	1.9	0.0005
6.34	1.8	0.0010
6.08	1.7	0.0015
5.37	0.8	0.0022
5.09	0.5	0.0005
4.56	0.9	0.0015
3.92	1.0	0.0005
3.39	1.7	0.0009
2.98	1.2	0.0045
1.20	N/A	N/A

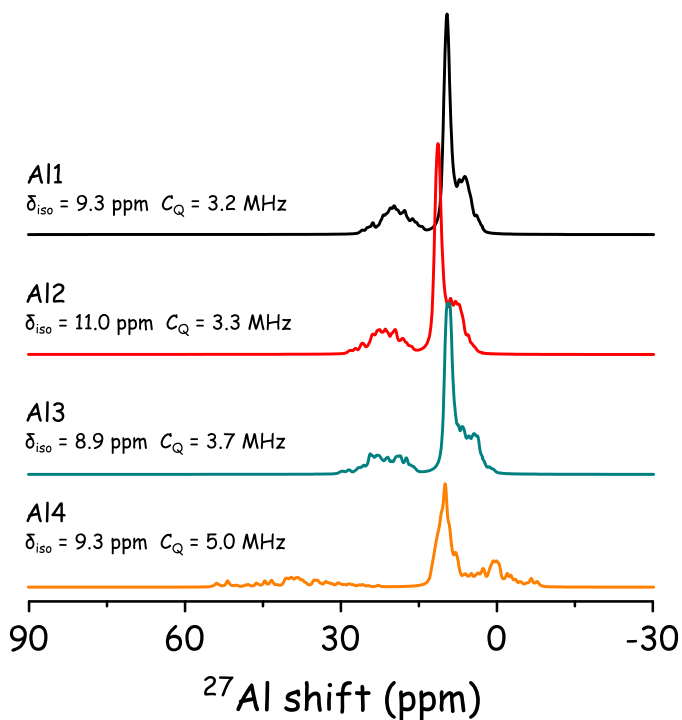


Figure S6. Numerical simulations⁴ of ^{27}Al spectra were recorded using $0.7 \mu\text{s}$ pulse length with rf-field strength of 250 kHz at $B_0 = 14.1 \text{ T}$ and a MAS frequency of 80 kHz. The simulated spectra illustrate the separation of the satellite transition from the Al4 site (30 – 50 ppm) from the other sites in agreement with the experiment in Fig. 9. Previously published ^{27}Al NMR data was used.⁵

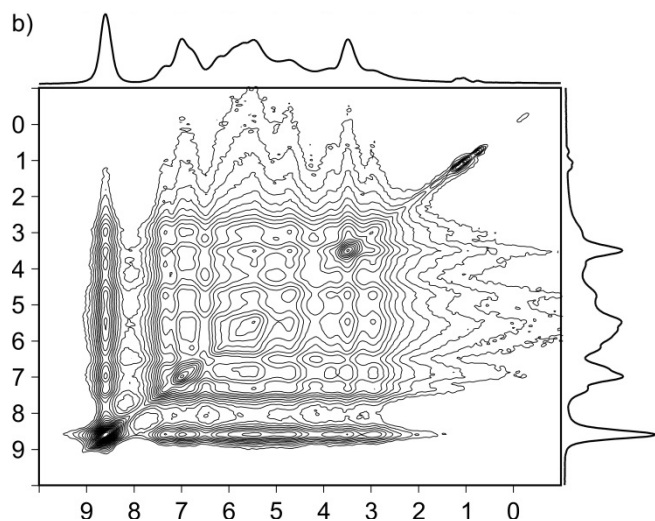


Figure S7. $^1\text{H}, ^1\text{H}$ NOESY with a 5 ms mixing time to probe long range correlations. The spectrum was recorded at 21.1 T with spinning speed of 80 kHz.

Table S4. The coordination of the OH groups.

	Metalion			Type:
H7	Al2	Al2	Zn	ZnAl ₂ -OH
H8	Al1	Al1	Zn	ZnAl ₂ -OH
H9	Al2	Al4	Zn	ZnAl ₂ -OH
H10	Al1	Al4	Zn	ZnAl ₂ -OH
H11	Al1	Al3		Al ₂ -OH
H12	Al3	Al4		Al ₂ -OH
H13	Al2	Al3	Zn	ZnAl ₂ -OH
H14	Al1	Al3	Zn	ZnAl ₂ -OH
H15	Al1	Al4		Al ₂ -OH
H16	Al2	Al3		Al ₂ -OH
H17	Al2	Al4		Al ₂ -OH
H18	Al3	Al4		Al ₂ -OH

Table S5. Correlation network

¹ H site (δ_{iso} (ppm))	Correlated ¹ H	Correlated ²⁷ Al	Assignment	
1.9(17)	%	%	Background	Not correlated with Al, hence not part of the MAI ₄ -LDH. Background
2.7(7)	3.8, 4.4, and 5.2	Al2 and Al4	H17	Al2 and Al4 bound => H9 or H17, ba like δ (Al ₂ OH) => H17
3.2(6)	3.8, 4.4, and 5.2	Al1/Al3, and Al4	H12	Al4 bound bayerite like δ (Al ₂ OH) => H12, H15 or H18. No 1H correlation to H17 => H12 or H15, 1H correlations to H16, the distance from H16 to H12 and H15 is 3.1 Å and 4.9 Å respectively => H12
3.8(6)	2.7, 3.2, 4.4, 5.2, and 5.9	Al1/Al3	H16	Al2 bound, bayerite-like δ (Al ₂ OH) => H16
4.4(8)	2.7, 3.2, 3.8	Al1/Al3, and Al4	H18 + water	Al4 bound, bayerite-like δ (Al ₂ OH) => H12, H15 or H18, 1H correlation to H17 observed => H18 (distance from H17 to H12, H15 and H18 is 3.1 Å, 4.9 Å, and 2.5 Å, respectively)
4.8(7)	2.7, 3.8, 6.5, 7.2 and 8.3	Al1/Al3	H11	Al1/Al3 bound, but bound to neither Al2 and Al4 and bayerite-like δ (Al ₂ OH) => H11 (only Al ₂ OH which is not bound to Al2 or Al4)
5.2(7)	2.7, 3.2, 3.8, 6.4 and 7.2		Water	
5.9(8)	2.7, 5.2, 7.2, 8.3	Al1/Al3, and Al2	H13 + water	Al2, but not Al4 bound, high δ (ZnAl ₂ OH) => H13 or H7, ¹ H correlation to H10 observed in 1 ms NOESY => H10 (H7-H10 distance 2.7 Å, H13-H10 distance 4.8 Å)
6.5(6)	7.2	Al1/Al3, and Al4	H15 + H8 or H14	Al4 and not Al2 bound, only not assigned Al4 bound H is H15 => H15
7.2(6)	4.8, 5.2, 6.5, and 8.3	Al1/Al3, Al2, and Al4	H9 + H8 or H14	Al2 and Al4 bound => H9 or H17, high δ (ZnAl ₂ OH) => H9
7.7(7)		Al1/Al3 and Al2	H7	Al2, but not Al4 bound, high δ (ZnAl ₂ OH) => H13 or H7, no ¹ H correlation to H10 observed in 1 ms NOESY => H7 (H7-H10 distance 2.7 Å, H13-H10 distance 4.8 Å)
8.3(5)	4.8, 5.9, 7.2 and 7.7	Al2, and Al4	H10	Al4 bound and high δ (ZnAl ₂ OH) => H10

Table S6. The calculated $\delta_{\text{iso}}(^1\text{H})$ (ppm) for $\text{ZnAl}_4\text{-SO}_4$. The calculated $\delta_{\text{iso}}(^1\text{H})$ are based the nickelalumite, where Ni have been replaced with Zn and the geometry has been optimised.³³ The DFT calculations were originally published in *Inorg. Chem.* 2016, 55, 9306-9015.³²

Site	$\delta_{\text{iso}}(^1\text{H})$ (ppm)
H ₂ O (H1-6)	6.2, 6.3, 6.6, 6.2, 7.8, and 4.5
H11	2.1
H12	2.6
H15	3.0
H10	3.4
H7	3.7
H9	5.0
H16	5.7
H18	8.2
H17	9.2
H14	10.1
H8	11.1
H13	11.4

References:

1. Uvarova, Y. A.; Sokolova, E.; Hawthorne, F. C.; Karpenko, V. V.; Agakhanov, A. A.; Pautov, L. A., The crystal chemistry of the "nickelalumite"-group minerals. *Can Miner.* **2005**, *43*, 1511-1519.
2. Britto, S.; Kamath, P. V., Polytypism in the Lithium-Aluminum Layered Double Hydroxides: The $[\text{LiAl}_2(\text{OH})_6]^+$ Layer as a Structural Syntho. *Inorg. Chem.* **2011**, *50*, 5619-5627.
3. Britto, S.; Kamath, P. V., Polytypism, Disorder, and Anion Exchange Properties of Divalent Ion (Zn, Co) Containing Bayerite-Derived Layered Double Hydroxides. *Inorg. Chem.* **2010**, *49*, 11370-11377.
4. Bak, M.; Rasmussen, J. T.; Nielsen, N. C., SIMPSON: A General Simulation Program for Solid-State NMR Spectroscopy. *J. Magn. Reson.* **2000**, *147*, 296-330.
5. Pushparaj, S. S. C.; Jensen, N. D.; Forano, C.; Rees, G. J.; Prevot, V.; Hanna, J. V.; Ravnsbæk, D. B.; Bjerring, M.; Nielsen, U. G., Structural Investigation of Zn(II) Insertion in Bayerite, an Aluminum Hydroxide. *Inorg. Chem.* **2016**, *55*, 9306-9315.